Adsorption of NO on the TiO_2(110) Surface: An Experimental and Theoretical Study

Dan C. Sorescu, Camelia N. Rusu, and John T. Yates, Jr.*

Surface Science Center, Department of Chemistry, University of Pittsburgh, Pittsburgh, Pennsylvania 15260

Received: October 18, 1999; In Final Form: February 16, 2000

The chemisorption properties of NO on the oxidized TiO_2(110) surface have been investigated using both experimental and theoretical methods. The results of temperature-programmed desorption measurements indicate that for NO exposures less than 1.1×10^{14} molecules/cm^2 NO adsorbs weakly and desorbs at ∼127 K. The thermal desorption kinetics are almost independent of the coverage of adsorbed NO molecules. The experimental activation energy for NO desorption from the nondefective TiO_2(110) surface is 8.4 kcal/mol in the limit of zero coverage. Above a critical NO surface exposure of 5.5×10^{14} molecules/cm^2, partial conversion of NO to N_2O is observed yielding N_2O desorption processes at ∼169 and ∼250 K. The weak interaction between the NO molecule and the TiO_2(110) surface has been also revealed from first-principles calculations based on density functional theory and the pseudopotential method in which NO molecules are adsorbed at the in-plane Ti cation sites. These calculations employ slab geometry and periodic boundary conditions with full relaxation of all atomic positions. As shown by the full relaxation of the atomic system, the most stable configuration of the NO molecule on the TiO_2(110) surface is tilted. There is a clear preference for the Ti−NO orientation compared to the Ti−ON configuration. At half coverage the adsorption energies of 10.52 and 5.75 kcal/mol have been determined for Ti−NO and Ti−ON binding configurations, respectively, in good agreement with the experimental results. At full coverage the adsorption energies were found to decrease by about 1.50−1.75 kcal/mol relative to the half-coverage case. The lack of large chemical effects indicates that the adsorption takes place through a predominantly physisorption mechanism. Besides the independent adsorption configurations of NO molecules, in the case of full coverage the formation of the N_2O_2 species was also observed theoretically. Among several different N_2O_2 isomers analyzed, the most stable has a *cis*-ONNO configuration with a binding energy of 13.6 kcal/mol in the singlet state. In addition to the bonding of NO, we also theoretically investigated different adsorption configurations of N_2O and NO_2 species on the TiO_2(110) surface. These studies indicate that for N_2O the most favorable adsorption configuration corresponds to a vertical Ti−N−N−O orientation with a binding energy of 7.73 kcal/mol at half coverage. In the case of the NO_2 molecule, a small binding energy of 2.11 kcal/mol was determined theoretically.

I. Introduction

The interactions between TiO_2 surfaces and a variety of molecules is a subject of particular importance in a number of surface-related applications such as catalysis, photocatalysis,[1−3] and sensor technology.[4] The adsorption of NO on TiO_2 surfaces is relevant for different technological applications such as pollution control, through catalytic reduction of NO, or for NO gas sensors.

In early experimental studies, Pande and Bell,[5] using temperature-programmed desorption (TPD) measurements, observed both NO and N_2O desorption from NO-exposed TiO_2 samples that were reduced at 523 K. They found that the yield of these products increased with increasing defect density. Further FT-IR studies[6] of NO adsorption on powdered TiO_2 indicated that NO adsorbs weakly on the fully oxidized TiO_2 surface at 300 K while on the reduced surface several molecular and dissociative adsorption states were identified. Rusu and Yates,[7] using FT-IR studies of NO adsorbed on reduced TiO_2 powders at 110 K, observed the formation of N_2O molecules with increased NO coverage.

Lu et al.[8] have studied the adsorption of NO on a single-crystal TiO_2(110) surface. It was found that on the annealed surfaces NO bonds weakly in a molecular adsorption state and desorbs at 120 K. Besides NO, N_2O was also formed as a reduction product. On the 400-K-annealed surface, N_2O was observed to desorb at ∼250 K. Increasing the annealing temperature causes the appearance of another N_2O desorption feature at ∼160 K. This low-temperature N_2O state, whose intensity is proportional to the surface defect coverage, was associated with NO reduction at surface oxygen vacancy sites. It has been suggested that a bridging-oxygen vacancy is involved in these processes.

In the present study we present a combined theoretical and experimental analysis of NO chemisorption on the TiO_2(110) surface. Several objectives have been addressed in the present work. First, accurate experimental data have been obtained on the adsorption properties of NO at low temperatures on the nominally defect-free surface. Second, we theoretically analyze the adsorption properties of the NO molecule on the TiO_2(110) surface, comparing the experimental findings with theoretical predictions. Finally, we analyze using theoretical means the main effects due to NO···NO interaction in the presence of the TiO_2 surface with the formation of N_2O_2 species.

II. Experimental Method

The experiments reported here were performed in a stainless steel vacuum (UHV) chamber described in detail elsewhere.[9−11] The base pressure in the UHV chamber is below 1×10^{-10}

10.1021/jp993694a CCC: $19.00
Published on Web 04/14/2000

Torr. The components of the chamber used to perform these experiments are (1) a shielded and apertured UTI 100C quadrupole mass spectrometer (QMS) for temperature-programmed desorption (TPD) measurements,[12] (2) a Perkin-Elmer digitally controlled cylindrical mirror analyzer (CMA) for Auger electron spectroscopy (AES) analysis, (3) an ion gun for Ar^+ sputter cleaning, (4) a low-energy electron diffraction (LEED) apparatus containing a dual microchannel plate detector for surface structural characterization, and (5) a collimated and calibrated microcapillary array doser for accurate gas exposure to the crystal surface.[13−16]

A polished ($10 \times 10 \times 1$ mm^3) TiO_2(110) single crystal was obtained from Princeton Scientific Corporation. The mounting procedure is described elsewhere.[17] The crystal was initially cleaned to remove C, Ca, and K traces by successive intervals of sputtering and annealing in UHV to 1000 K. The nearly perfect oxidized surface was obtained by rapidly annealing the clean crystal to 900 K in a flux (1.1×10^{13} molecules/s·cm^2) of $^{16}O_2$, followed by cooling in the O_2 beam and by continuous exposure to this flux at room temperature for 6 h. This surface presented a sharp (1×1) LEED pattern and an Auger spectrum characteristic of clean TiO_2.

The temperature of the crystal was measured with a type K thermocouple cemented into a precut slot at one corner of the crystal using a high-temperature ceramic adhesive.[17] The thermocouple feedback to the temperature controller[18] permitted linear programming of the temperature of the crystal at a constant rate of 0.5 K/s.

The surface was dosed with isotopically labeled nitric oxide (^{15}NO) through the microcapillary array collimated beam doser. The conductance of the beam doser was governed by an internal pinhole aperture. The beam doser was calibrated with N_2 using standard volumetric methods.[14] On the basis of the geometrical arrangement of the crystal, the flux of the ^{15}NO molecules intercepted by the crystal is 2.2×10^{13} molecules/Torr·s·cm^2.

Isotopically labeled ^{15}NO was obtained from Cambridge Isotope Laboratories and was purified by freeze−pump−thaw cycles. The isotopic purity was 99.0% ^{15}N.

III. Computational Method

The computational method employed in the present study is similar to that we have previously used to analyze the adsorption properties of CO on the TiO_2(110) surface.[19] Basically, the periodic nature of the surface is considered in the present simulations by the aid of a tridimensional model. Within this model, the surface is simulated by supercells repeated periodically in all three directions. Repetition of the simulation box in the plane of the slab creates an infinite slab, while periodicity in the direction perpendicular to the slab creates an infinite stack of slabs. By separating each slab from its neighbors by a vacuum layer, the otherwise unphysical interactions between slabs in a direction perpendicular to the surface are made negligible. This approach has been found to be very useful to study the energetics of perfect crystals, lattice defects, and surfaces for a number of oxides including TiO_2.[19−23] It was also employed in several static and dynamical studies of molecular adsorption on different surfaces, such as water adsorption on the TiO_2(110) surface.[24−26]

The calculations performed in this study were done using the CETEP code,[27] the parallel version of CASTEP (Cambridge Serial Total Energy Package).[28] This program evaluates the total energy of periodically repeating geometries based on density-functional theory and the pseudopotential approximation. In this case only the valence electrons are represented explicitly in the calculations, the valence−core interaction being described by nonlocal pseudopotentials. Periodic boundary conditions are used with the occupied electronic orbitals expanded in a plane-wave basis. The expansion includes all plane waves whose kinetic energy $\hbar^2K^2/2m < E_{cut}$, where K is the wave vector, m the electronic mass, and E_{cut} the chosen cutoff energy. This cutoff energy is chosen to ensure the convergence with respect to the basis set. A spin-polarized gradient-corrected form of the exchange correlation functional (GGS) was used in the manner suggested by White and Bird.[29] It was previously shown[29,30] that the GGA approximation gives more accurate results for the energetics of molecular adsorption than the local density approximation (LDA). The Brillouin zone was sampled with the lowest-order Monkhorst-Pack[31] set of two k-points, with the component parallel to the surface normal set to zero.

The pseudopotentials used in this study are norm-conserving of the form suggested by Kleinman and Bylander[32] and optimized using the scheme of Lin et al.[33] The pseudopotentials for Ti and O are those we have previously used for investigation of CO adsorption on the TiO_2(110) surface.[19] Briefly, the Ti 3p states and all lower states of the Ti atom, as well as the O 1s states, are treated as core states. The Ti pseudopotential was generated from the neutral atom for s and d components, while for the p component the configuration $4s^{0.75}4p^{0.25}3d^2$ was used. The core radii were 2.2, 2.7, and 2.2 bohr for s, p, and d waves, respectively. The oxygen pseudopotential was generated using the $2s^22p^4$ configuration for the s and p waves and the configuration $2s^22p^{2.75}3d^{0.25}$ for the d wave, with a core radius of 1.5 bohr for all components. The N pseudopotential was generated using the $2s^22p^3$ configuration for the s and p waves and the configuration $2s^12p^{1.75}3d^{0.25}$ for the d wave, with core radii 1.0, 1.4, and 1.4 bohr for s, p, and d waves, respectively.

The self-consistent ground state of the system was determined using an all-bands conjugate gradient technique to minimize the total energy of the system with respect to the plane-wave coefficients. The optimization of different atomic configurations reported in this study was done using the Broyden−Fletcher−Goldfarb−Shanno (BFGS) minimization technique, with an energy threshold of 1.0×10^{-6} eV for the ground-state search.

IV. Results and Discussion

A. Experimental Results for ^{15}NO Adsorption on Oxidized TiO_2(110) Surface. *1. ^{15}NO Adsorption on TiO_2(110) Oxidized Surface.* Adsorption of ^{15}NO at 118 K was carried out on an oxidized TiO_2(110) surface over an exposure range from 1.1×10^{13} molecules/cm^2 to 4.4×10^{15} molecules/cm^2. Preoxidation of TiO_2 (110) has been shown to lower the O-anion vacancy defect level.[8,34] The thermal desorption spectra for ^{15}NO ($m/e = 31$), for different NO exposures, are presented in Figure 1. NO adsorbs weakly and nondissociatively on the oxidized TiO_2 surface and desorbs at ∼127 K. For NO exposures higher than 5.5×10^{14} molecules/cm^2 an additional peak appeared at ∼169 K. A second additional desorption peak (∼250 K) begins to develop for NO exposures above 2.2×10^{15} molecules/cm^2. The desorption peaks observed at ∼169 and ∼250 K are cracking products from $^{15}N_2O$ desorption and correlate with $^{15}N_2O^+$ ($m/e = 46$) desorption (not shown). This desorption behavior is in good agreement with the results obtained by Lu et al.[8]

Figure 2 shows the NO thermal desorption yield as a function of increasing NO exposure. It summarizes the fact that for exposures smaller or equal to 5.5×10^{14} molecules/cm^2, NO desorbs nondissociatively from the surface and only for exposures larger than this value, part of the NO is converted to N_2O. For NO exposures larger than this critical value, NO molecules mutually interact to form N_2O.

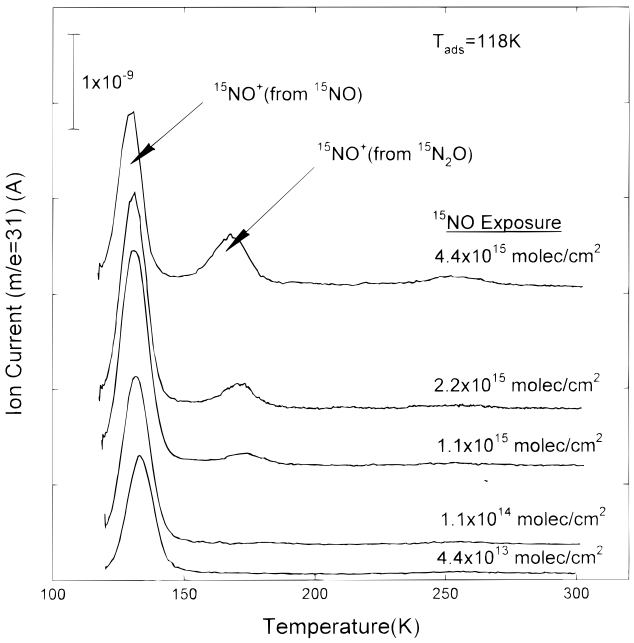

Figure 1. Temperature-programmed desorption spectra for ^{15}NO from the fully oxidized $TiO_2(110)$ surface. The ^{15}NO exposures displayed range from 4.4×10^{13} to 4.4×10^{15} molecules/cm^2.

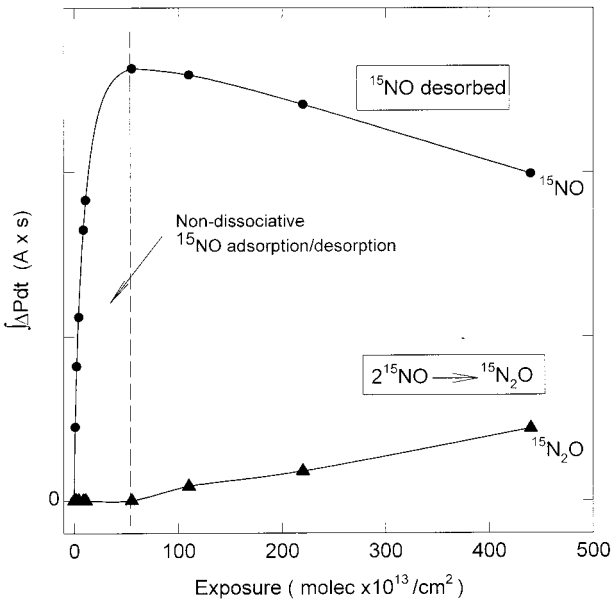

Figure 2. ^{15}NO and $^{15}N_2O$ thermal desorption yields as a function of the ^{15}NO exposure of the oxidized $TiO_2(110)$.

In the coverage range where N_2O forms, the yield of NO exhibits a complementary decrease. We attribute this behavior to the increasing probability for N_2O production due to NO••NO interactions at higher NO coverages. Lateral interaction between the NO molecules at high coverages causing an increase in the N_2O yield was also seen for NO adsorbed on ZnO-$(10\bar{1}0)$.[35]

2. Activation Energy for Desorption. Temperature-programmed desorption spectra for ^{15}NO from the fully oxidized $TiO_2(110)$ surface for exposures smaller or equal to 5.5×10^{14} molecules/cm^2, corresponding only to the nondissociative desorption process, are shown in Figure 3.

To determine the kinetic parameters of the desorption, the first-order desorption process was modeled by using the Runge−Kutta method. The kinetic parameters found for first-order kinetics are $E_d = 8.4$ kcal/mol and $\nu_1 = 3 \times 10^{13}$ s^{-1}, and the quality of fit to one TPD peak is shown in the inset to Figure 3. The small observed downward shift of 2 K for increasing coverage corresponds to a decrease in the activation energy of desorption of 0.2 kcal/mol over the observed coverage range.

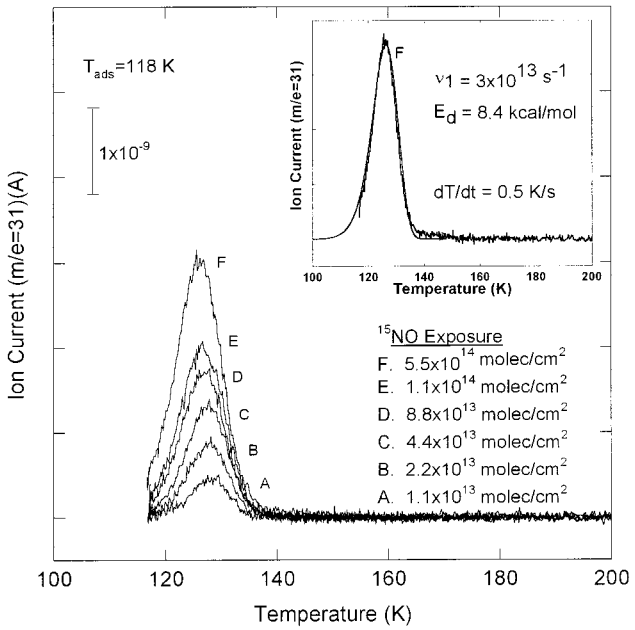

Figure 3. Temperature-programmed desorption spectra for ^{15}NO from the fully oxidized $TiO_2(110)$ surface. The inset shows the first-order kinetic fit achieved for $E_d = 8.4$ kcal/mol and $\nu = 3 \times 10^{13}$s^{-1}.

B. Tests of the Computational Method. The accuracy of the theoretical method employed here has been first tested by considering the optimization of bulk TiO_2, of the bare surface, and of a number of isolated molecular species, i.e., NO, N_2O, NO_2, and several N_2O_2 isomers, which might be involved in the process of adsorption. The detailed description of the bulk and slab optimizations results have been described previously,[19] and the tests performed for optimization of free molecular species are given in the Appendix. Here we will summarize only the main results of these tests.

The optimized lattice parameters for tetragonal bulk rutile are $a = 4.6760$ Å and $c = 3.0027$ Å, with the internal coordinates $u = 0.3045$. The errors relative to experimental values[36] of cell dimensions a and c are 1.78% and 1.51% at cutoff energy $E_{cut} = 850$ eV, while the corresponding error for the internal parameter u is 0.15%. At this plane-wave cutoff, the total energy of the TiO_2 unit cell is convergent to within 0.04 eV.

We have modeled the TiO_2 surface as infinite slabs of material. This was obtained by performing calculations with periodic boundary conditions on a stack of slabs, each one being separated from its neighbors by a vacuum layer (see Figure 4). The surface unit cell has dimensions of $\sqrt{2}a \times c$ along $[\bar{1}10]$ and [001] directions, where a and c are the crystallographic dimensions of the bulk TiO_2 unit cell. In the present calculations we used a slab containing three layers with all the bridging oxygen atoms on the surface present. This slab contains three O−(Ti−O−Ti−O)−O plane units, corresponding to 6 Ti atoms and 12 O atoms. The vacuum separation width was chosen equal to 6.8 Å, value that is slightly greater than twice the separating distance between the O−(Ti−O−Ti−O)−O units. Both our[19] and previous studies[24,25] showed that such a vacuum separation width is enough to ensure that interactions between neighboring slabs were small.

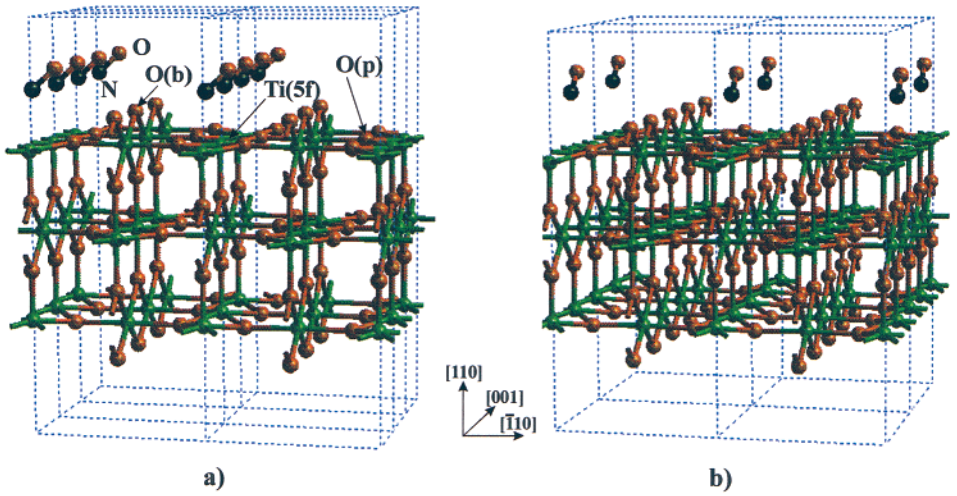

Figure 4. 1 × 1 (left panel) and 1 × 2 (right panel) slab configurations used to study the adsorption of NO on the TiO_2(110) surface at full and. respectively, half coverages. The different types of surface atoms are indicated as follows: Ti(5f) 5-fold-coordinated titanium, Ti(6f) 6-fold-coordinated titanium, O(b) bridging-oxygen atom, and O(p) in-plane oxygen.

The results of the relaxation of the TiO_2(110) surface presented in detail in our earlier study[19] indicate significant displacements of the surface atoms, particularly along the [110] direction. The calculated values of these displacements were found similar to those determined in X-ray diffraction measurements[37] as well as to the previous LDA results.[22] Also, the calculated surface energy of 0.79 J/m^2 was in close agreement with the values reported by Goniakowski et al.[30] based on the Perdew−Wang and Becke−Perdew forms of the GGA exchange correlation.

Finally, the calculations performed on an isolated NO molecule that are presented in the Appendix indicate that a good convergence of the molecular energy can be obtained at a cutoff energy of 850 eV. For this cutoff energy the predicted equilibrium NO distance is found in very good agreement with the experimental value[38] with a difference of only 0.0038 Å (0.28%). The calculations performed for one NO molecule isolated in a box of different lengths indicate that for intermolecular NO···NO distances larger than 5 Å the interactions between molecules become negligible. Similarly, the predicted equilibrium configurations of N_2O and NO_2 molecules are found to be very close to the experimental structures,[39,40] with maximum bond deviations from the experimental values of 1.59% and 1.84%, respectively. Finally, for both the singlet and triplet symmetric *cis*-ONNO and cyclic NONO species, the calculated structures are found to be very close to previous DFT and MCSCF results.[41,42] Besides the geometrical agreement, we find that for both the symmetric and asymmetric *cis*-N_2O_2 configurations, the triplet state is slightly lower than the corresponding singlet state, by 1.8 and 1.6 kcal/mol, respectively, in good agreement with previous DFT theoretical findings.[41]

The totality of the results performed in these tests indicate that our theoretical approach is able to give a good description for the bulk TiO_2, for the bare surface, and for the isolated molecules of interest. This fact allows us to proceed confidently to the next stage represented by theoretical investigation of NO adsorption on the TiO_2(110) surface.

C. Theoretical Results for NO Adsorption on TiO_2(110). *1. Adsorption of NO Molecule at Ti(5f) Sites.* The adsorption of NO was investigated by performing calculations in which the entire system molecule−substrate is relaxed to equilibrium with the NO molecule adsorbed on the TiO_2(110) surface at the 5-fold-coordinated Ti sites. The dependence of the adsorption

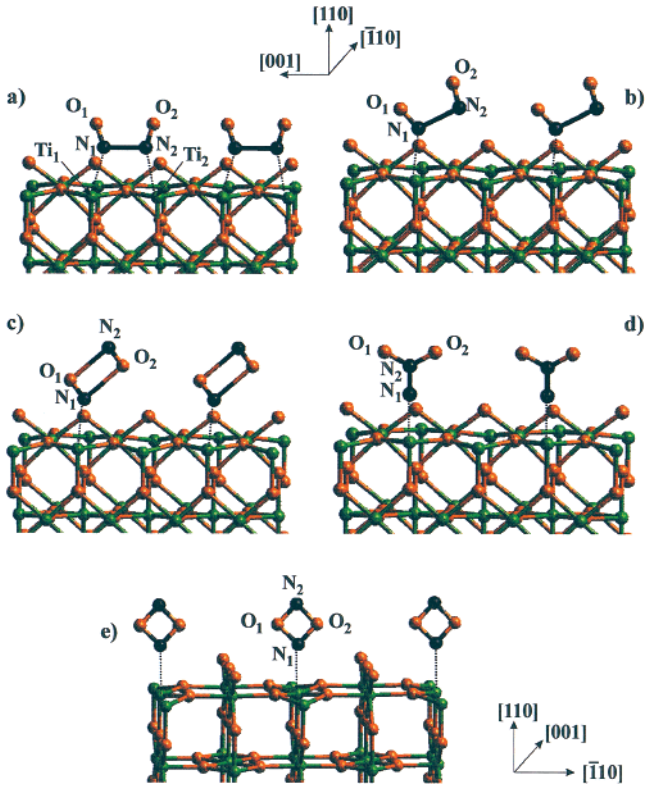

Figure 5. (a) Symmetric and (b) asymmetric adsorption configurations of symmetric *cis*-N_2O_2, and the adsorption configurations of (c) asymmetric *cis*-N_2O_2, (d) dioxirane-like NNOO isomers on the TiO_2-(110) surface, and (e) cyclic NONO.

energies on NO coverages was investigated using both 1 × 1 (see Figure 5a) and 1 × 2 (see Figure 5b) supercells. In the latter case, the slab is doubled along the [001] direction and contains twice as many atoms as the 1 × 1 slab. The calculations were performed with each repeating cell containing a single or two NO molecules in the case of 1 × 2 supercell, which are placed on one of the surfaces of the slab. Thus NO coverages of $\theta = 1$ and $\theta = 0.5$ can be studied with these models. For both coverages we have investigated two molecular configurations of the NO molecule, i.e., with the N atom and with the O atom oriented toward the surface.

For all configurations considered we calculated the adsorption energies according to the expression

$$E_{ads} = (NE_{molec} + E_{slab} - E_{tot})/N \quad (1)$$

where E_{molec} is the energy of the isolated NO molecule in its equilibrium position, E_{slab} is the total energy of the slab, E_{tot} is the total energy of the adsorbate/slab, system, and N is the total number of NO molecules in the unit cell, i.e., $N = 1$ or 2. A positive E_{ads} corresponds to a stable adsorbate/slab system. In calculating the energies of the bare slab and of the molecule−slab systems, the same Brillouin-zone sampling has been used.

The calculated binding energies of NO molecule with the two orientations are given in Table 1. We have determined that the most stable configurations correspond to a tilted geometry in which the N atom is oriented toward the surface. In the case of full-coverage calculations performed in the 1×1 unit cell, the Ti−NO orientation is favored by about 5.0 kcal/mol compared to the Ti−ON configuration. The corresponding equilibrium distances are 2.354 Å for Ti−N versus 2.532 Å for Ti−O, respectively, with similar tilted angles of 134.0° for Ti−N−O and 131.8° for Ti−O−N, respectively.

Owing to the fact that in the case of 1×1 surface unit cell the intermolecular distances between the neighbor NO molecules are below the 5 Å limit (in which the intermolecular interactions are not negligible), it is important to analyze the dependence of the adsorption results on the size of the unit cell. We have performed such investigations by considering a 1×2 unit cell in which the slab is doubled along the [001] direction. For this case we have considered two situations: one with a single NO molecule per cell ($\theta = 0.5$) and the other one with two NO molecules that are not correlated by translational symmetry ($\theta = 1.0$).

As can be seen in Table 1, the adsorption energies at half coverage are increased by 1.5 kcal/mol for Ti−NO and by 1.75 kcal/mol for Ti−ON configurations relative to the results obtained in the 1×1 unit cell. In this case the most stable configurations are obtained when the NO molecule is situated in the $(\bar{1}10)$ plane (see entry 4 in Table 1). However, the potential energy in this region is very shallow, and other equilibrium configurations, out of the $(\bar{1}10)$ plane, are also possible (see entry 5 in Table 1).

An interesting situation has been observed in the case when two NO molecules per 1×2 unit cell have been considered. In the case when both NO molecules are positioned in the $(\bar{1}10)$ plane above the Ti(5f) sites (see Figure 5b), the molecules adsorb at about 2.42 Å with a binding energy of 8.25 kcal/mol for the triplet state or 7.86 kcal/mol for the singlet state. However, in those situations when the molecules are positioned out of the $(\bar{1}10)$ plane, the molecules interact with each other leading to formation of the *cis*-N_2O_2 compound (see Figure 5a).

2. Adsorption of N_2O_2 molecules at Ti(5f) Sites. For the *cis*-N_2O_2 species we have identified two adsorption configurations: a symmetrical (Figure 5a) and an asymmetrical (Figure 5b) one relative to the Ti(5f) sites. The highest adsorption energy of 13.67 kcal/mol was determined for the symmetrical configuration of N_2O_2 in the singlet state. Similar adsorption configurations have been obtained for N_2O_2 in the triplet state. However, in this case the most stable configuration is asymmetrical with an adsorption energy of 6.34 kcal/mol.

The presence of the *cis*-N_2O_2 species on the $TiO_2(110)$ surface raises the question if other N_2O_2 structural isomers cannot be adsorbed on this surface. To answer this question we have considered the adsorption of the asymmetric NONO, dioxirane-like NNOO isomers, and cyclic NONO (see Figures 5c,d,e). These cases have been simulated only in the 1×2 surface cell, and the corresponding results are indicated in Table 1. We find that the adsorption energy for the asymmetric *cis*-NONO molecules in the singlet state is 11.56 kcal/mol, slightly smaller than the corresponding adsorption energy for symmetric *cis*-ONNO structure. Also, the cyclic NONO isomer is adsorbed in a tilted geometry, symmetrical relative to the $(\bar{1}10)$ plane, with an adsorption energy of 8.98 kcal/mol. Finally, the NNOO isomer is adsorbed vertically above the Ti(5f) sites with a binding energy of 9.21 kcal/mol. These results indicate that the most stable configuration among different N_2O_2 isomers is *cis*-ONNO but other configurations, particularly the asymmetric NONO, are also possible.

As our experimental results indicate the formation of N_2O species with the increase of NO coverage ($>5.5 \times 10^{14}$ molecules/cm^2), we believe that this reaction might involve the decomposition of N_2O_2 species. Such a reaction mechanism has been shown to be valid in the gas phase by Nguyen et al.[43] using large-scale multireference configuration interaction wave function calculations. In addition, our preliminary calculations indicate that another reaction path for the formation of N_2O on the $TiO_2(110)$ surface might be represented by the reaction of N_2O_2 with a oxygen vacancy defect site. A more detailed analysis of this process will be the subject of a future study.[44]

3. Adsorption of N_2O and NO_2 Species. As mentioned in the Introduction, previous experimental studies[5,8] have presented evidence for the existence of N_2O species on the annealed TiO_2-(110) surface. Consequently, we have extended our analysis to molecular species other than NO, particularly to N_2O and NO_2 molecules. The geometrical parameters of these two molecules are indicated in Table 1 together with the corresponding adsorption energies.

In the case of the N_2O molecule we have analyzed both configurations, with N and with O atoms toward the surface. At half coverage we found that both adsorption configurations are vertical, the Ti−N−N−O configuration being more stable by about 3.6 kcal/mol than the reverse Ti−O−N−N geometry. Moreover, there is a significant decrease of the adsorption energy of N_2O species with increasing coverage, owing to repulsion between neighbor molecules.

In the case of NO_2, the adsorption energy is quite small, about 2.1 kcal/mol, and consequently this species will not exist on the surface except at very low temperatures. In summary, the most probable adsorption configurations of NO, particularly at low coverages, correspond to Ti−NO binding. The corresponding adsorption energy we have found in the half-coverage case is about 10.5 kcal/mol. This value is also supported by the experimental values reported in this study. Despite the fact that we have not done calculations at coverages smaller than 0.5, we have shown above that the intermolecular NO−NO interactions are small enough for this particular configuration such that the value of 10.5 kcal/mol determined in this work should be a close approximation of the binding energy in the limit of zero coverage.

4. Frequency Calculations for NO Molecules. Another point we have investigated theoretically is the shift of the N−O vibrational frequency as the result of the adsorption process on the cationic sites of the $TiO_2(110)$ surface. For this purpose we have determined the NO stretching frequency for the Ti−NO adsorption configuration using a frozen-phonon approach. Particularly, we have determined the total energy of several configurations in which the N and O atoms were moved along N−O bond direction such that the center of mass of the NO molecule remained fixed. The vibrational frequency has been calculated from a polynomial interpolation of the variation of

TABLE 1: Calculated Equilibrium Distances and Angles and the Corresponding Adsorption Energies for the NO, NO_2, N_2O Molecules and N_2O_2 Isomers on TiO_2(110) Surface as Function of the Coverage Θ[a]

system/model	Θ	bond lengths (Å)				bond angles (deg)		E_{ads} (kcal/mol)
1. $TiO_2(1\times1)+NO^{v}$	1.0	$r_{(Ti-N)}$	2.319	$r_{(N-O)}$	1.140	$\theta_{(Ti-N-O)}$	180.0	6.15
2. $TiO_2(1\times1)+NO^{t}$	1.0	$r_{(Ti-N)}$	2.354	$r_{(N-O)}$	1.136	$\theta_{(Ti-N-O)}$	134.0	9.08
3. $TiO_2(1\times1)+ON^{t}$	1.0	$r_{(Ti-O)}$	2.532	$r_{(N-O)}$	1.147	$\theta_{(Ti-O-N)}$	131.8	4.07
4. $TiO_2(1\times2)+NO^{t,*}$	0.5	$r_{(Ti-N)}$	2.428	$r_{(N-O)}$	1.128	$\theta_{(Ti-N-O)}$	130.2	10.52
5. $TiO_2(1\times2)+NO^{t,**}$	0.5	$r_{(Ti-N)}$	2.403	$r_{(N-O)}$	1.127	$\theta_{(Ti-N-O)}$	129.0	10.50
6. $TiO_2(1\times2)+ON^{t,**}$	0.5	$r_{(Ti-O)}$	2.567	$r_{(N-O)}$	1.138	$\theta_{(Ti-N-O)}$	126.7	5.75
7. $TiO_2(1\times2)+2(NO)^{t,*,tr}$	1.0	$r_{(Ti-N1)}$	2.419	$r_{(N1-O1)}$	1.134	$\theta_{(Ti-N1-O1)}$	134.6	8.25
		$r_{(Ti-N2)}$	2.423	$r_{(N2-O2)}$	1.135	$\theta_{(Ti-N2-O2)}$	134.9	
8. $TiO_2(1\times2)+2(NO)^{t,*,sg}$	1.0	$r_{(Ti-N1)}$	2.383	$r_{(N1-O1)}$	1.133	$\theta_{(Ti-N1-O1)}$	136.4	7.86
		$r_{(Ti-N2)}$	2.383	$r_{(N2-O2)}$	1.133	$\theta_{(Ti-N2-O2)}$	136.4	
9. $TiO_2(1\times2)+N_2O_2$ (sym-cis-tr)^{s}	1.0	$r_{(Ti-N1)}$	2.662	$r_{(N1-O1)}$	1.143	$\theta_{(Ti-N1-O1)}$	144.9	6.34
		$r_{(Ti-N2)}$	2.673	$r_{(N2-O2)}$	1.143	$\theta_{(Ti-N1-O1)}$	145.3	
				$r_{(N1-N2)}$	1.995			
10. $TiO_2(1\times2)+N_2O_2$ (sym-cis-tr)^{as}	1.0	$r_{(Ti-N1)}$	2.417	$r_{(N1-O1)}$	1.153	$\theta_{(Ti-N1-O1)}$	134.6	7.62
		$r_{(Ti-N2)}$	3.449	$r_{(N2-O2)}$	1.127	$\theta_{(Ti-N1-O1)}$	159.0	
				$r_{(N1-N2)}$	2.090			
11. $TiO_2(1\times2)+N_2O_2$ (sym-cis-sg)^{s}	1.0	$r_{(Ti-N1)}$	2.335	$r_{(N1-O1)}$	1.141	$\theta_{(Ti-N1-O1)}$	147.5	13.67
		$r_{(Ti-N2)}$	2.334	$r_{(N2-O2)}$	1.141	$\theta_{(Ti-N1-O1)}$	147.5	
				$r_{(N1-N2)}$	1.920			
12. $TiO_2(1\times2)+N_2O_2$ (sym-cis-sg)^{as}	1.0	$r_{(Ti-N1)}$	2.308	$r_{(N1-O1)}$	1.150	$\theta_{(Ti-N1-O1)}$	134.6	10.55
		$r_{(Ti-N2)}$	3.552	$r_{(N2-O2)}$	1.127	$\theta_{(Ti-N1-O1)}$	176.3	
				$r_{(N1-N2)}$	2.023			
13. $TiO_2(1\times2)+N_2O_2$ (asym-cis-sg)^{as}	0.5	$r_{(Ti-N1)}$	2.318	$r_{(N1-O1)}$	1.148	$\theta_{(Ti-N1-O1)}$	132.1	11.56
				$r_{(N2-O2)}$	1.120	$\theta_{(O1-N1-O2)}$	85.7	
				$r_{(N1-O2)}$	2.342	$\theta_{(N1-O2-N2)}$	93.0	
				$r_{(N2-O1)}$	2.315	$\theta_{(O2-N2-O1)}$	87.6	
						$\theta_{(N2-O1-N1)}$	93.6	
14. $TiO_2(1\times2)+NONO$	0.5	$r_{(Ti-N1)}$	2.399	$r_{(N1-O1)}$	1.363	$\theta_{(Ti-N1-O1)}$	132.8	8.98
				$r_{(N1-O2)}$	1.361	$\theta_{(O1-N1-O2)}$	88.6	
				$r_{(N2-O1)}$	1.358	$\theta_{(N1-O2-N2)}$	91.3	
				$r_{(N2-O2)}$	1.360	$\theta_{(O2-N2-O1)}$	88.8	
						$\theta_{(N2-O1-N1)}$	91.3	
15. $TiO_2(1\times2)+NNOO$	1.0	$r_{(Ti-N1)}$	2.087	$r_{(N1-N2)}$	1.235	$\theta_{(N1-N2-O1)}$	118.5	9.21
				$r_{(N2-O1)}$	1.253	$\theta_{(O1-N2-O2)}$	122.9	
				$r_{(N2-O2)}$	1.253			
16. $TiO_2(1\times2)+N_2O^{v}$	1.0	$r_{(Ti-N1)}$	2.441	$r_{(N1-N2)}$	1.106	$\theta_{(Ti-N1-N2)}$	176.7	3.77
				$r_{(N2-O)}$	1.175			
17. $TiO_2(1\times2)+N_2O^{v}$	0.5	$r_{(Ti-N1)}$	2.401	$r_{(N1-N2)}$	1.106	$\theta_{(Ti-N1-N2)}$	177.1	7.73
				$r_{(N2-O)}$	1.173			
18. $TiO_2(1\times2)+ON_2^{v}$	0.5	$r_{(Ti-O)}$	2.831	$r_{(N1-N2)}$	1.104	$\theta_{(Ti-O-N2)}$	175.1	4.18
				$r_{(O-N2)}$	1.186			
19. $TiO_2(1\times2)+NO_2^{v}$	0.5	$r_{(Ti-N)}$	2.923	$r_{(N-O1)}$	1.196	$\theta_{(O1-N-O2)}$	134.5	2.11
				$r_{(N-O2)}$	1.197			

[a] Notations NO and ON pertain to the orientations of the NO molecule on the rutile surface, i.e., with N and O atoms toward the surface. The superscript abbreviations used are v, vertical configuration; t, tilted configuration, *, configuration in $(\bar{1}10)$ plane; **, configuration out of $(\bar{1}10)$ plane. The other abbreviations are sym, symmetrical; asym, asymmetrical; tr, triplet state; sg, singlet state; s, symmetrical bound on two Ti(5f) sites; as, asymmetrically bound on a single Ti(5f) site; and O(b), the bridging oxygen site.

total energy with the interatomic N−O distance. For the isolated gas-phase NO molecule, a vibrational frequency of 1793 cm^{-1} has been determined. This value is about 4.3% smaller than the experimental value of 1875 cm^{-1}.[38] This level of agreement is typical of GGA calculations and is adequate for present purposes. In the case of NO adsorption on the TiO_2(110) surface, we have considered only the Ti−NO geometry at half coverage (see Figure 4b). For this configuration a vibrational frequency of 1797 cm^{-1} was found. These results indicate a very small shift of the vibrational frequency of the NO molecule as result of adsorption. At the present moment, we are not aware of experimental results for the vibrational frequency of NO on the oxidized rutile surface to allow a comparison with the above findings.

5. Bonding Mechanism. Further insight into the type of bonding mechanism for NO and *cis*-N_2O_2 molecules on the TiO_2(110) surface can be obtained by analyzing the distribution of the electron density in the molecule−slab system. In Figures 6a and 7a we present a contour plot of the electron densities in a plane perpendicular to the (110) surface which passes through the middle of the N−O bond distance(s). In these figures, the [110] direction corresponds to the vertical axis while the horizontal axis is parallel to the $[00\bar{1}]$ direction. As can be seen in both figures, the valence electron density is highly concentrated on N and O atoms of the NO and N_2O_2 molecules and on O atoms of the slab while Ti atoms are invisible. The adsorption of NO and N_2O_2 molecules does not introduce significant changes of the electron distributions.

An additional procedure to determine the effect of molecular adsorption on the electron distribution can be obtained by evaluating the difference electron density maps. These can be calculated by subtracting from the electron density of the adsorbent−adsorbate system the electron densities of both the TiO_2(110) slab and the NO (N_2O_2) isolated molecules, with the relative atomic position corresponding to the adsorbed configuration. These differential maps are indicated in Figures 6b and 7b. In the case of NO adsorption, the main distortion effects are localized on the adsorption sites with a small contribution of the O atoms below the Ti(5f) site. When adsorption occurs there is a clear polarization of the NO molecule, with an increase

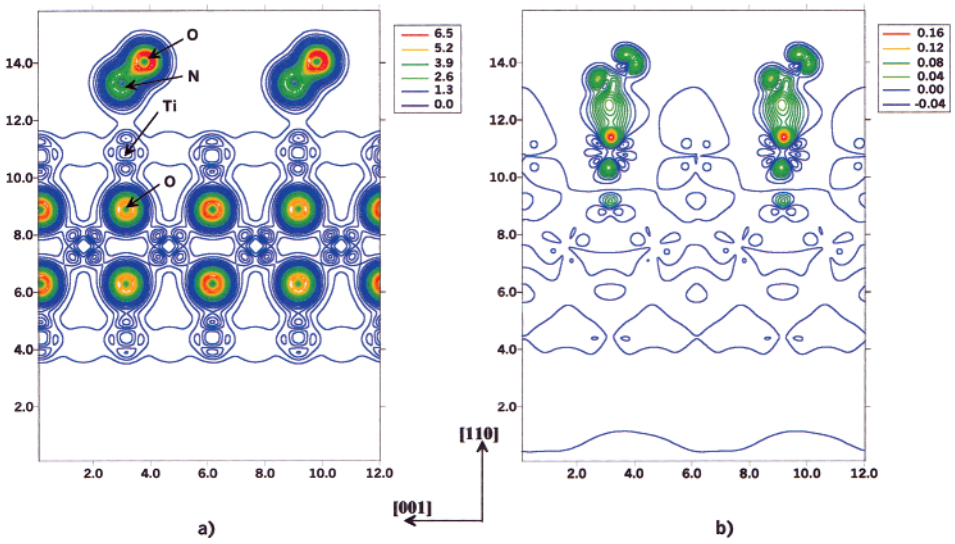

Figure 6. Contour plot of the valence electron density (units of electrons/Å^3) (a) and of the difference between the electron density shown in (a) and the one resulting from the superposition of the TiO_2(110) slab and the isolated NO molecule (b) in the case of Ti−NO adsorption at half coverage. The contours are taken along the ($\bar{1}$10) plane containing the NO molecules and the surface Ti(5f) sites. The [110] direction is parallel to the vertical axis.

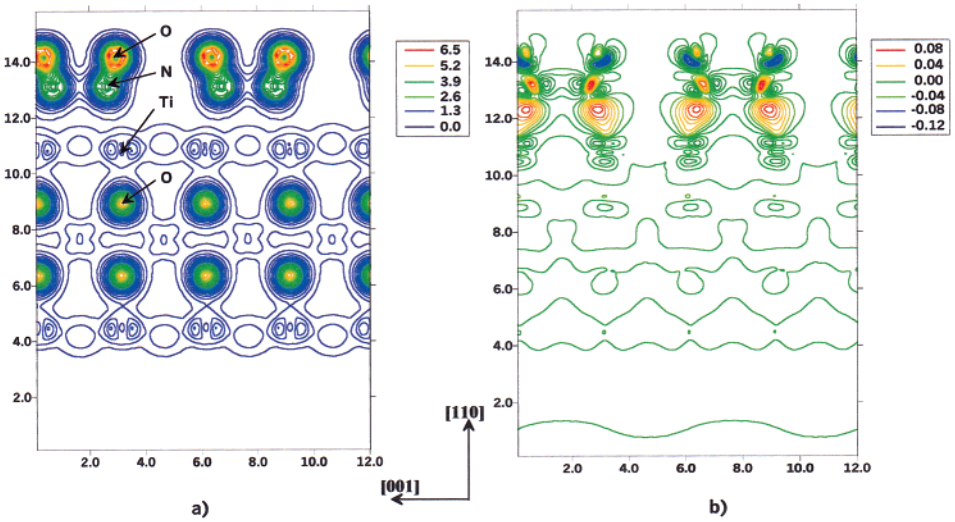

Figure 7. Contour plot of the valence electron density (units of electrons/Å^3) (a) and the difference between the electron density shown in (a) and the one resulting from the superposition of the TiO_2(110) slab and the isolated N_2O_2 molecule (b) in the case of Ti−N_2O_2 adsorption at full coverage. The contours are taken along a plane parallel to the ($\bar{1}$10) plane passing through the middle of N−O bond distances. The [110] direction is parallel to the vertical axis.

of the electronic charge in the region between the nitrogen and titanium atoms. These effects can be understood as being due to a superposition of a polarization mechanism under the surface electric field and an incipient σ-donation process from NO to the 5-fold Ti site. In the case of N_2O_2 adsorption, a similar increase of the electron density between the N and Ti(5f) atoms can be seen. In addition a depletion of charge on oxygen atoms of N_2O_2 is accompanied by a corresponding positive accumulation on nitrogen atoms of the same molecule. The small distortion effects observed for these two configurations indicate a predominant electrostatic attraction of the NO and N_2O_2 molecules to the surface. These findings are also supported by small modifications of the equilibrium geometries relative to gas-phase configurations and by small adsorption energies.

V. Conclusions

We have performed both experimental and theoretical studies to investigate the adsorption of NO on the TiO_2(110) oxidized surface. The following conclusions have been reached from this investigation:

(1) Molecular NO adsorbs weakly on the oxidized TiO_2(110) surface and desorbs at ∼127 K.

(2) For low coverages of NO ($<5.5 \times 10^{14}$ molecules/cm^2) on oxidized TiO_2(110) at 118 K, NO desorbs nondissociatively. For higher coverages ($>5.5 \times 10^{14}$ molecules/cm^2), NO is partly converted to N_2O.

(3) The first-order desorption kinetic analysis of the NO adsorbed on the oxidized TiO_2(110) yields $E_d = 8.4$ kcal/mol and $\nu = 3 \times 10^{13}$ s^{-1} at saturation NO coverage.

(4) The calculated adsorption energies based on DFT theory and a pseudopotential model indicate that at Ti(5f) sites the preferred adsorption configuration corresponds to a Ti−NO type of bonding and this configuration is bent.

(5) The calculated adsorption energies vary from 9.08 (4.07) kcal/mol to 10.52 (5.75) kcal/mol for Ti−NO (Ti−ON) configurations when the coverage is decreased from 1 to $^1/_2$.

TABLE 2: Comparison of Calculated and Experimental Bond Lengths, *r*, Bond Angles, *θ*, of Different Gas-Phase Molecules Considered in the Present Study[a]

molecule	cell length *L* (Å)	geometry	*r* (Å)	exptl	total energy (eV)
NO	4	$r_{(N-O)}$	1.1470		−703.184 508
	5	$r_{(N-O)}$	1.1473		−703.164 870
	6	$r_{(N-O)}$	1.1474		−703.161 618
	8	$r_{(N-O)}$	1.1475		−703.161 943
	10	$r_{(N-O)}$	1.1475	1.1508[c]	−703.161 943

molecule	geometry	*r* (Å)[b]		exptl/calcd	*θ* (deg)[b]	exptl/calcd
N_2O	$r_{(N-N)}$	1.109	1.127[d]	$\theta_{(N-N-O)}$	180.0	180.0
	$r_{(N-O)}$	1.184	1.185[d]			
NO_2	$r_{(N-O)}$	1.199	1.194[e]	$\theta_{(O-N-O)}$	133.7	134.1[e]
N_2O_2 (sym-cis-sing)	$r_{(N-N)}$	2.014	2.237[f]	$\theta_{(O-N-N)}$	105.5	99.6[f]
	$r_{(N-O)}$	1.150	1.161[f]			
N_2O_2 (sym-cis-sing)	$r_{(N-N)}$		1.987−2.119	$\theta_{(O-N-N)}$		99.6−97.6
LCGTO-DF[g]	$r_{(N-O)}$		1.161−1.174			
N_2O_2 (sym-cis-triplet)	$r_{(N-N)}$	2.006	2.237[f]	$\theta_{(O-N-N)}$	110.1	99.6[e]
	$r_{(N-O)}$	1.150	1.161[d]			
N_2O_2 (sym-cis-triplet)	$r_{(N-N)}$		1.875−2.059	$\theta_{(O-N-N)}$		109.2−111.1
LCGTO-DF[g]	$r_{(N-O)}$		1.166−1.176			
N_2O_2 (asym-cis-sing)	$r_{(N1-O1)}$	1.144		$\theta_{(O1-N1-O2)}$	85.4	
	$r_{(N1-O2)}$	2.358		$\theta_{(N1-O2-N2)}$	93.9	
	$r_{(N2-O2)}$	1.144		$\theta_{(O2-N2-O1)}$	86.1	
	$r_{(N2-O1)}$	2.345		$\theta_{(N2-O1-N1)}$	94.6	
NONO	$r_{(N1-O1)}$	1.367	1.3651[h]	$\theta_{(O2-N1-O1)}$	87.9	87.62[h]
	$r_{(N1-O2)}$	1.367		$\theta_{(N1-O1-N2)}$	92.0	92.38[h]
	$r_{(N2-O2)}$	1.366		$\theta_{(O1-N2-O2)}$	88.0	
	$r_{(N2-O1)}$	1.367		$\theta_{(N2-O2-N1)}$	92.0	
NNOO	$r_{(N1-N2)}$	1.250		$\theta_{(O1-N2-O2)}$	125.7	
	$r_{(N2-O1)}$	1.252				
	$r_{(N2-O1)}$	1.252				

[a] In the case of the NO molecule we indicate also the dependence of the results on the dimension *L* of a periodic box with sides $L \times 10 \times 10$ Å^3. The direction of NO bond is perpendicular to box direction denoted by *L*. The other results have been determined in the (1×2) periodic box of the TiO_2(110) Surface used in slab calculations. [b] Calculated in the present study. [c] Reference 38. [d] Reference 39. [e] Reference 40. [f] Reference 45. [g] Results of linear combination of Gaussian-type orbitals-density functional (LCGTO−DF) from ref 41. [h] MCSCF results from ref 42.

The value calculated for Ti−NO is in excellent agreement with the experimental measurement of 8.4 kcal/mol. We have shown that for distances larger than 5 Å the intermolecular NO−NO interactions are practically negligible. Consequently, it is expected that the binding energy in the limit of zero coverage is close to the value determined in the present study for the half-coverage case. The small modification of the NO bond length as result of adsorption as well as the small changes of the valence electron distribution indicate that the predominant mechanism for NO bonding to the TiO_2(110) surface is through electrostatic interactions. This is verified by the small shift in ν_{NO} upon adsorption.

(6) In the case of full coverage or when the distance between NO molecules becomes smaller than 3 Å, the interaction between NO molecules may lead to formation of N_2O_2 species. The configuration with the highest adsorption energy of 13.67 kcal/mol was found to be symmetrically bounded from two adjacent Ti(5f) sites.

(7) The configurations and adsorption energies of different isomeric forms of N_2O_2 have been investigated. In all cases weak adsorption energies between 8 and 10 kcal/mol have been determined.

(8) Other molecular species such as N_2O or NO_2 are very weakly bonded on the TiO_2(110) surface, with adsorption energies of 7.73 and 2.11 kcal/mol, respectively.

Acknowledgment. We thank Professor M. C. Payne at Cavendish Laboratory, Cambridge, U.K. for allowing us to use the CETEP code. We are also grateful for allocations of time on the Cray T3E at Pittsburgh Supercomputer Center. We thank the Army Research Office for support of this work.

Appendix. Calculations on Free NO, N_2O, and NO_2 Molecules and N_2O_2 Isomers

The accuracy of the pseudopotentials used in this work have been also tested by calculations of the equilibrium properties of isolated molecules NO, N_2O, and NO_2 and of different N_2O_2 isomers, species that can be involved in the adsorption of NO on the TiO_2 surface. First, we present in Table 2 the results of geometry optimization for the NO molecule in an orthorhombic repeating cell with dimensions $L \times 10 \times 10$ Å^3, where $L = 4-10$ Å, and for the cutoff energy of 850 eV. In these calculations a single *k*-point at the Γ-point has been used.

The analysis of the results for increasing lengths of the dimension *L* indicates a negligible intermolecular interaction for a length larger than 5 Å. For example, the increase of the length *L* from 5 to 10 Å causes a variation of only 0.003 eV of the total energy of the molecule. In addition, there is a very small variation of the equilibrium bond distance of NO, which varies between 1.1473 and 1.1475 Å for cell lengths larger than 5 Å. These values agree very well with the experimental bond distance of 1.1508 Å.[38] A similar good correspondence has been obtained for the other molecular species. For example, the calculated bond lengths and angles differ from the corresponding experimental results by less than 1.59% for N_2O and 1.84% for NO_2.

Special attention has been given in this study to the N_2O_2 dimeric forms of NO. This species has been identified in both

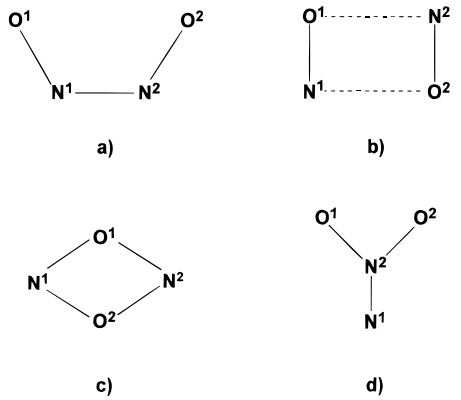

Figure 8. N_2O_2 structural isomers investigated in this study: (a) symmetric *cis*-N_2O_2; (b) asymmetric *cis*-N_2O_2; (c) cyclic NONO; (d) dioxirane-like NNOO.

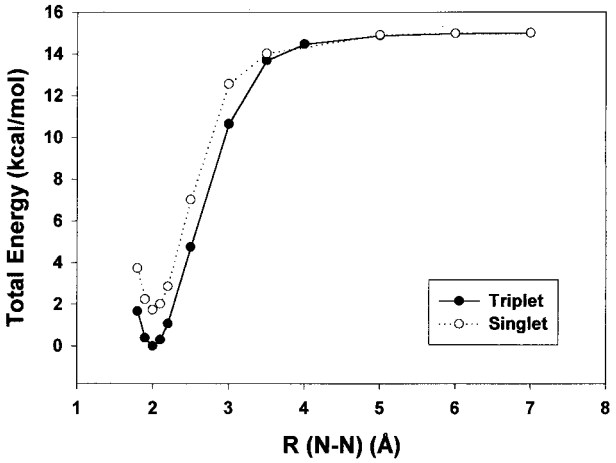

Figure 9. Total energy variation as function of the N···N intermolecular distance between two NO molecules.

condensed phase[46,47] and gas phase.[45] The experimental data suggest that the most stable configuration has C_{2v} symmetry with an N−N linkage (see Figure 8), but other isomeric forms presented here have been also proposed and characterized theoretically.[31,48] It is important to remark that the equilibrium geometries predicted for these species[41,48] show a significant dependence on the type of theoretical correlation treatment. For this reason we present in Table 2 the results predicted by our theoretical analysis as well as by the previous theoretical studies based on a linear combination of Gaussian-type orbitals−density functional (LCGTO−DF)[41] method. As can be seen in Table 2 the sets of equilibrium values predicted in our calculations are in good correspondence with the other sets of theoretical values.

A problem of intense debate emphasized in previous studies[41,48] is that of the relative positions of the singlet and triplet states for *cis*-ONNO isomers. In the present study we have considered this issue by investigating these states for both symmetric and asymmetric *cis*-N_2O_2 isomers. Our results indicate that the triplet state for both these isomers is more stable by 1.7 and 1.6 kcal/mol, respectively, than the singlet state. These results agree with the previous DFT data obtained using a variety of different functionals, namely, Vosko−Wilk−Nussair (VWN), Becke−Perdew (BP) and Perdew−Wang (PW).[43] These methods predict for triplet−singlet energy difference values between 2.8 and 3.9 kcal/mol.

Another test we have considered in the present study is the variation of the total energy for a system of two NO molecules as a function of the distance between their N−N atoms. The corresponding variation is represented in Figure 9. These results have been obtained by optimizing the positions of O atoms of the two NO molecules while the N atoms were kept fixed at specific positions. These calculations have been done in a periodic box with larger dimensions, i.e., $18 \times 10 \times 10$ Å. The two NO molecules are initially oriented parallel to each other, with their N−O axes perpendicular to the N−N direction. The N−N axis is parallel to the longest side of the box cell. As can be seen in Figure 9, for N−N distances larger than 5 Å the interaction between molecules is practically negligible. Below 5 Å there is a stabilization of the total energy corresponding to an attractive interaction between the two NO molecules up to an equilibrium distance of 2.014 Å for the singlet state and of 2.006 Å for the triplet state. For N−N distances below these values, the interactions between the two molecules become repulsive.

References and Notes

(1) Fox, M. A.; Dulay, M. T. *Chem. Rev.* **1993**, 93, 341.
(2) Henrich, V. E.; Cox, P. A. *The Surface Science of Metal Oxides*, Cambridge University Press: Cambridge, England, 1993.
(3) Linsebigler, A. L.; Lu G.; Yates, J. T., Jr. *Chem. Rev.* **1995**, *95*, 735.
(4) Huusko, J.; Lantto, V.; Torvela, H. *Sens. Actuators* **1993**, *B15*−*16*, 245.
(5) Pande, N. K.; Bell, A. T. *J. Catal.* **1986**, *97*, 137.
(6) Boccuzzi, F.; Guglielminotti, E.; Spoto, G. *Surf. Sci.* **1991**, *251*, 1069.
(7) Rusu, C. N.; Yates, J. T., Jr. *J. Phys. Chem. B* **2000**, *104*, 1729.
(8) Lu, G.; Linsebigler, A. L.; Yates, J. T., Jr. *J. Phys. Chem.* **1994**, *98*, 11733.
(9) Lu, G.; Linsebigler A. L.; Yates, J. T., Jr. *J. Vac. Sci. Technol., A* **1994**, *12* (2), 384.
(10) Linsebigler, A. L,; Lu, G.; Yates, J. T., Jr. *Surf. Sci.* **1993**, *294*, 284.
(11) Hanley, L.; Guo, X.; Yates, J. T., Jr. *J. Chem. Phys.* **1989**, *91*, 7220.
(12) Smentkowski, V. S.; Yates, J. T. Jr., *J. Vac. Sci. Technol., A* **1989**, *7*, 3325.
(13) Bozack, M. J.; Muehlhoff, L. J.; Russell, J. N., Jr.; Choyke, W. J.; Yates, J. T., Jr. *J. Vac. Sci. Technol., A* **1987**, *5*, 1.
(14) Winkler, A.; Yates, J. T., Jr. *J. Vac. Sci. Technol., A* **1988**, *6*, 2929.
(15) Campbell, C. T.; Valone, S. M. *J. Vac. Sci. Technol., A* **1985**, *3*, 408.
(16) Linsebigler, A. L.; Smentkowski, V. S.; Ellison, M. D.; Yates, J. T., Jr. *J. Am. Chem. Soc.* **1992**, *14*, 465.
(17) Lu, G.; Linsebigler, A. L.; Yates, J. T., Jr. *J. Chem. Phys.* **1995**, *102*, 4657.
(18) Muha, R. J.; Gates, S. M.; Basu, P.; Yates, J. T., Jr. *Rev. Sci. Instrum.* **1985**, *56*, 613.
(19) Sorescu, D. C.; Yates, J. T., Jr. *J. Phys. Chem.* **1998**, *B23*, 4556.
(20) Glassford, K. M.; Chelikowsky, J. R. *Phys. Rev. B* **1992**, *46*, 1284.
(21) Ramamoorthy, M.; King-Smith, R. D.; Vanderbilt, D. *Phys. Rev.* **1994**, *B49*, 7709.
(22) Ramamoorthy, M.; Vanderbilt, D.; King-Smith, R. D. *Phys. Rev.* **1994**, *B49*, 16721.
(23) Lindan, P. J. D.; Harrison, N. M.; Holender, J. M.; Gillan, M. J.; Payne, M. C. *Surf. Sci.* **1996**, *364*, 431.
(24) Lindan, P. J. D.; Harrison, N. M.; Holender, J. M.; Gillan, M. J. *Chem. Phys. Lett.* **1996**, *261*, 246.
(25) Lindan, P. J. D.; Muscat, J.; Bates, S., Harrison, N. M.; Gillan, M. J. *J. Chem. Soc., Faraday Trans.* **1998**, *106*, 135.
(26) Lindan, P. J. D.; Harrison, N. M.; Gillan, M. J. *Phys. Rev. Lett.* **1998**, *80*, 762.
(27) Clarke, L. J.; Štich, I.; Payne, M. C. *Comput. Phys. Commun.* **1992**, *72*, 14.
(28) Payne, M. C.; Allan, D. C.; Arias, T. A.; Johannopoulus, J. D. *Rev. Mod. Phys.* **1992**, *64*, 1045.
(29) White, J. A.; Bird, D. M.; Payne, M. C.; Štich, I. *Phys. Rev. Lett.* **1994**, *73*, 1404.
(30) Goniakowski, J.; Holender, J. M.; Kantorovich, L. N.; Gillan, M. J.; White, J. A. *Phys. Rev.* **1996**, *B53*, 957.
(31) Monkhorst, H. J.; Pack, J. D. *Phys. Rev.* **1976**, *B13*, 5188.
(32) Kleinman, L.; Bylander, D. M. *Phys. Rev. Lett.* **1980**, *45*, 566.
(33) Lin, J. S.; Qteish, A.; Payne, M. C.; Heine, V. *Phys. Rev.* **1993**, *B47*, 4174.
(34) Rusu, C. N.; Yates, J. T., Jr. *Langmuir* **1997**, *13*, 4311.
(35) Zwicker, G.; Ranke, W.; Jacobi, K.; Pöss, D. *Ber. Bunsen-Ges. Phys. Chem.* **1984**, *88*, 364.

(36) Wyckoff, R. W. G. *Crystal Structures*, 2nd. ed; Wiley: Interscience: New York, 1964; Vol. 1.

(37) Charlton, G.; Howes, P. B.; Nicklin, C. L.; Steadman, P.; Taylor, J. S. G.; Muryn, C. A.; Harte, S. P.; Mercer, J.; McGrath, R.; Norman, R. D.; Turner, T. S.; Thornton, G. *Phys. Rev. Lett.* **1997**, *78*, 495.

(38) Huber, K. P.; Herzberg G. *Molecular Spectra and Molecular Structure*, *Vol. 4: Constants of Diatomic Molecules*; Van Nostrand: Princeton, NJ, 1979.

(39) Teffo, J. L.; Chédin, A. *J. Mol. Spectrosc.* **1989**, *135*, 389.

(40) Hardwick, J. L.; Brand, J. C. D. *Can. J. Phys.* **1976**, *54*, 80.

(41) Stirling, A.; Pápai, I.; Mink, J.; Salahub, D. R. *J. Chem. Phys.* **1994**, *100*, 2910.

(42) Nguyen, K. A.; Gordon, M. S.; Montgomery, J. A., Jr.; Michels, H. H. J. *Phys. Chem.* **1994**, *98*, 10072.

(43) Nguyen, K. A.; Gordon, M. S.; Montgomery, J. A., Jr.; Michels, H. H.; Yarkony, D. R. *J. Chem. Phys.* **1993**, *98*, 3845.

(44) Sorescu, D. C.; Rusu, C. N.; Yates, J. T., Jr. *J. Phys. Chem.*, to be published.

(45) Kukolich, S. G. *J. Mol. Spectrosc.* **1983**, *104*, 4715.

(46) Laane, J.; Ohlsen, J. R. *J. Am. Chem. Soc.* **1978**, *100*, 6948.

(47) During, J. R., Griffen, M. G. *J. Raman Spec.* **1976**, *5*, 273.

(48) Lee, T. J.; Rice, J. E.; Scuseria, G. E.; Schaefer, H. F., III. *Theor. Chim. Acta* **1989**, *75*, 81.